Journal of Solid State Chemistry 183 (2010) 866–870

Contents lists available at ScienceDirect

Journal of Solid State Chemistry

journal homepage: www.elsevier.com/locate/jssc

Verwey-type transition within the $Pb_3Rh_{7-x}Mn_xO_{15}$ solid solution

Alvin J. Gatimu, Hiroshi Mizoguchi, Arthur W. Sleight, M.A. Subramanian *

Department of Chemistry, Oregon State University, Corvallis, OR 97331, USA

ARTICLE INFO

Article history:
Received 19 December 2009
Received in revised form
4 February 2010
Accepted 10 February 2010
Available online 16 February 2010

Keywords:
Oxides
Lead
Rhodium
Manganese
Verwey-type transition

ABSTRACT

A complete solid solution was found between isostructural $Pb_3Mn_7O_{15}$ and $Pb_3Rh_7O_{15}$. Single-crystals of two members of the solid solution $Pb_3Rh_{7-x}Mn_xO_{15}$ (x=1.07 and 2.26) were grown and their crystal structures were determined. The Verwey-type transition for $Pb_3Rh_7O_{15}$ at 185 K remains with a 3% substitution of Mn for Rh but disappears with 4% substitution of Mn for Rh. The magnetic ordering temperature found for $Pb_3Mn_7O_{15}$ at about 70 K is maintained at a 43% substitution of Rh for Mn but has disappeared for 57% substitution of Rh for Mn. The unit cell volume of this layered structure contracts with increasing x for $Pb_3Rh_{7-x}Mn_xO_{15}$ phases, but the structure actually expands in the direction perpendicular to the layers due to increased separation between the layers.

1. Introduction

The same basic structure is found for both $Pb_3Mn_7O_{15}$ and $Pb_3Rh_7O_{15}$ (Fig. 1), and apparently no other compounds have been synthesized with this structure [1–7]. Structural studies establish that all Pb is 2+ in both the compounds, thus, there is mixed valency of Rh and Mn with an average oxidation state of 3.4+. There are four or more crystallographic sites for the Rh or Mn atoms. Bond valence calculations indicate some charge ordering of M^{3+} and M^{4+} cations for both $Pb_3Mn_7O_{15}$ and $Pb_3Rh_7O_{15}$, but a complete description of this charge ordering has been elusive for both the compounds. The high electrical conductivity and magnetic properties of $Pb_3Rh_7O_{15}$ indicate some delocalization of the 4*d* electrons of Rh whereas the magnetic properties of $Pb_3Mn_7O_{15}$ indicate a lack of such delocalization for the 3*d* electrons of Mn [7,8]. The dielectric properties of $Pb_3Mn_7O_{15}$ have suggested possible interesting multiferroic properties for this compound [9].

The ideal structures for both $Pb_3Mn_7O_{15}$ and $Pb_3Rh_7O_{15}$ are hexagonal. However, the first structure determination for $Pb_3Mn_7O_{15}$ by Darriet et al. concluded that the actual symmetry at room temperature is orthorhombic [1]. The orthorhombic description was later supported by Marsh et al. [2]. Le Page et al. subsequently argued that this structure is really hexagonal [3]. A very recent high resolution study by Rasch et al. using synchrotron data resolved this controversy in favor of orthorhombic symmetry [4]. The lattice of $Pb_3Mn_7O_{15}$ is metrically far from hexagonal at 15 K. With increasing temperature the lattice metrically approaches hexagonal, but is still not quite metrically hexagonal by 295 K [4].

The structure of $Pb_3Rh_7O_{15}$ at room temperature is clearly hexagonal with a space group of $P6_3/mcm$ [5–7]. However, there is a phase transition at 185 K. The space group changes below this phase transition, but extensive efforts have failed to reveal the correct space group below 185 K [7]. High resolution diffraction studies using synchrotron data show no detectable metric deviation from a hexagonal lattice down to 80 K [7]. Electrical conductivity and other measurements indicate that the transition for $Pb_3Rh_7O_{15}$ at 185 K is a Verwey-type transition with a change in charge ordering associated with Rh [7]. The primary motivation of this study was to examine the impact on this transition as Mn is substituted for Rh.

2. Experimental

Reactants were PbO (99.9% Aldrich), Rh_2O_3 prepared from RhI_3 by heating in air at 1073 K for 10 h, and Mn_2O_3 (98% Johnson Matthey). Stoichiometric amounts of the oxides were ground under ethanol in an agate mortar and pestle. Pelletized samples were placed in an alumina boat and heated to 1073 K for Rh rich samples and 1148 K for Mn rich samples. X-ray powder diffraction data were collected with a RIGAKU MINIFLEX II using Cu$K\alpha$ radiation and a graphite monochromator.

Single crystals of composition $Pb_3Rh_{5.93}Mn_{1.07}O_{15}$ and $Pb_3Rh_{4.74}Mn_{2.26}O_{15}$ were grown in a PbO flux in an intimate mixture of PbO, Rh_2O_3 and Mn_2O_3 in a 1:10 and 1:5 sample:PbO excess ratio, respectively. Crystal growth was observed in a Pt

* Corresponding author. Fax: +1 541 737 2062.
E-mail address: mas.subramanian@oregonstate.edu (M.A. Subramanian).

0022-4596/$ - see front matter © 2010 Elsevier Inc. All rights reserved.
doi:10.1016/j.jssc.2010.02.008

crucible heated to 1373 K in air for 10 h then cooled to 1223 K at 3 K/h. After holding at 1223 K for 0.5 h, the crucible was cooled to room temperature at 200 K/h. Excess flux was dissolved in HNO_3 (aq) at up to 473 K. Black plate-like crystals resulted with dimensions of up to 0.134×0.097 mm and 0.061×0.048 mm for the $Pb_3Rh_{5.93}Mn_{1.07}O_{15}$ and $Pb_3Rh_{4.74}Mn_{2.26}O_{15}$ compositions, respectively.

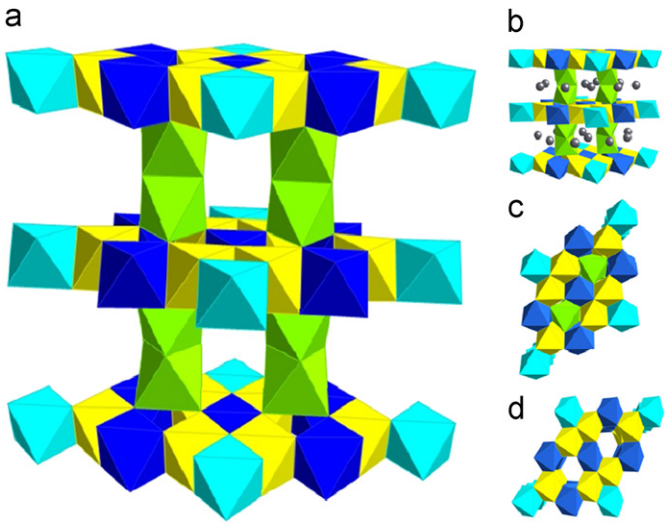

Fig. 1. Structure of $Pb_3Rh_7O_{15}$ and $Pb_3Mn_7O_{15}$. Colors of octahedra indicate Rh valencies in $Pb_3Rh_7O_{15}$. Green represents Rh^{3+} in the 8*h* site, yellow represents $Rh^{3.5+}$ in the 12*i* site, cyan represents Rh^{3+} in the 2*b* site, and dark blue represents Rh^{4+} in the 6*f* site. (b) The hexagonal structure with the Pb atoms shown in two sites within the interlayer region. (c) A view along the *c*-axis of the structure with the interlayer Rh present and (d) without the interlayer Rh present. (For interpretation of the references to color in this figure caption, the reader is referred to the web version of the article.)

Single-crystal X-ray diffraction data for $Pb_3Rh_{5.93}Mn_{1.07}O_{15}$ and $Pb_3Rh_{4.74}Mn_{2.26}O_{15}$ were collected at 173 and 233 K respectively using a Bruker SMART APEXII CCD system and an Oxford Cyrostream Cooler. A fine focus tube was used with an anode power of 50 KV at 30 mA, a crystal to plate distance of 6.0 cm, 512×512 pixels/frame, beam center (256.52, 253.16), ϕ/ω scan with step of 0.30°, exposure/frame of 10.0 s/frame, and SAINT integration. An absorption correction was applied by SADABS. Crystal structures were solved by direct methods and refined with full-matrix least-squares method using the SHELXTL package. Further measurements to higher angles were carried out using an Oxford-Diffraction Xcalibure2 CCD diffractometer equipped with a Cryojet cooling device.

Electrical conductivity measurements were conducted by the conventional four-probe method over the temperature region 60–300 K. Magnetic susceptibility data were obtained with a Quantum Design PPMS ACMS magnetometer using a field of 0.5 T.

3. Results

All $Pb_3Rh_{7-x}Mn_xO_{15}$ compositions attempted yielded single phase products suggesting a complete solid solution between $Pb_3Mn_7O_{15}$ and $Pb_3Rh_7O_{15}$. Fig. 2 shows the variation in the unit cell edges, *c*/*a* ratio, and unit cell volume for the $Pb_3Rh_{7-x}Mn_xO_{15}$ phases based on refinement of powder XRD data. Crystallographic results for $Pb_3Rh_{5.93}Mn_{1.07}O_{15}$ and $Pb_3Rh_{4.74}Mn_{2.26}O_{15}$ single crystals are summarized in Table 1. The refined atomic coordinates are given in Table 2, and the refined Rh/Mn occupations are in Table 3. The compositions of $Pb_3Rh_{5.93}Mn_{1.07}O_{15}$ and $Pb_3Rh_{4.74}Mn_{2.26}O_{15}$

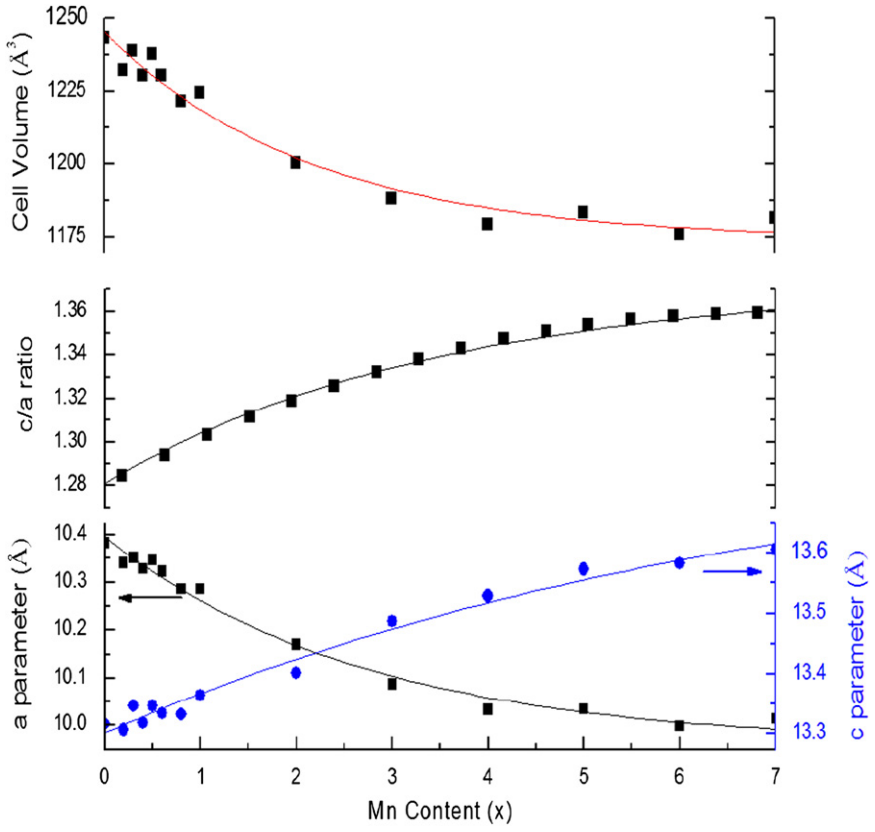

Fig. 2. Cell edges, *c*/*a*, and unit cell volume for $Pb_3Rh_{7-x}Mn_xO_{15}$ phases.

are based on these occupation refinements. The c/a value of 1.32 for the $Pb_3Rh_{4.74}Mn_{2.26}O_{15}$ crystal fits well on the c/a plot (Fig. 2) providing independent verification of the composition. Some interatomic distances are given in Table 4 and plotted vs. composition in Fig. 3. Further crystallographic details may be found in available cif files.

Table 1
Summary of crystallographic results.

Empirical formula	$Pb_3Rh_{5.93}Mn_{1.07}O_{15}$	Pb_3 $Rh_{4.74}Mn_{2.26}O_{15}$
Formula weight	1530.85	1473.65
Temperature	173(2) K	233(2) K
Wavelength	0.71073 Å	0.71073 Å
Crystal system	Hexagonal	Hexagonal
Space group	$P6_3/mcm$	$P6_3/mcm$
Unit cell dimensions	a=10.260(1) Å	a=10.150(2) Å
	c=13.342(3) Å	c=13.387(5) Å
Volume	1216.3(4) Å3	1194.3(5) Å3
Z	4	4
Density (calculated)	8.360 g/cc	8.196 g/cc
Absorption coefficient	50.345/mm	50.883/mm
F(000)	2639	2543
Crystal size	0.05 × 0.03 × 0.01 mm	0.05 × 0.04 × 0.02 mm
Theta range for data collection	2.29–26.99°	2.32–27.00°
Index ranges	$-13 \le h \le 13$, $-13 \le k \le 13$, $-17 \le l \le 16$	$-12 \le h \le 12$, $-12 \le k \le 12$, $-17 \le l \le 17$
Reflections collected	12 491	12 309
Independent reflections	515 [R(int)=0.0585]	504 [R(int)=0.0523]
Completeness to theta=28.24°	100.00%	100.00%
Absorption correction	Semi-empirical from equivalents	SADABS
Max. and min. transmission	0.6329 and 0.1874	0.4293 and 0.1852
Refinement method	Full-matrix least-squares on F^2	Full-matrix least-squares on F^2
Data/restraints/parameters	515/4/59	504/4/59
Goodness-of-fit on F^2	1.182	1.165
Final R indices [$I > 2\sigma(I)$]	$R1$=0.0172, w$R2$=0.0395	$R1$=0.0162, w$R2$=0.0346
R indices (all data)	$R1$=0.0186, w$R2$=0.0404	$R1$=0.0176, w$R2$=0.0356
Extinction coefficient	0.00008(2)	0.00107(4)
Largest diff. peak and hole	1.317 and −1.654 e/Å^3	1.061 and −1.176 e/Å^3

Results of our four-probe electrical resistivity measurements on sintered polycrystalline bars are shown vs. temperature in Fig. 4. Resistivity values are normalized to 1.0 at room temperature to eliminate variations due to variable porosity and grain boundary contributions. The room temperature resistivities of $Pb_3Mn_7O_{15}$ and $Pb_3Rh_7O_{15}$ are 360 and 0.001 Ω cm, respectively. Results of our magnetic susceptibility measurements for Mn-rich compositions using Curie-Weiss fitting are presented in Table 5 and Fig. 5.

4. Discussion

Given that Mn^{3+} and Mn^{4+} are smaller than Rh^{3+} and Rh^{4+}, respectively, we can expect that the average M–O distances for the MO_6 octahedra will decrease with increasing Mn content for the $Pb_3Rh_{7-x}Mn_xO_{15}$ phases. This is, in fact, the trend observed for

Table 3
Site percentage (%) occupied by Rh for the four octahedral sites.

	Position	$Pb_3Rh_{5.93(2)}Mn_{1.07(2)}O_{15}$	$Pb_3Rh_{4.74(2)}Mn_{2.26(2)}O_{15}$
M	All	84.7	67.7
M1	8h	96.6	89.3
M2	12i	79.0	55.5
M3	2b	77.2	49.9
M4	6f	82.3	66.0

Table 4
Interatomic distances in Å.

	$Pb_3Rh_7O_{15}$	$Pb_3Rh_{5.93}Mn_{1.07}O_{15}$	$Pb_3Rh_{4.74}Mn_{2.26}O_{15}$
Pb1–O3 × 4	2.654(4)	2.667(4)	2.657(4)
Pb1–O4 × 2	2.403(6)	2.395(6)	2.379(6)
Pb1–O4 × 2	3.105(5)	3.080(5)	3.057(5)
Pb2–O1 × 2	2.384(5)	2.407(7)	2.435(5)
Pb2–O4 × 2	2.353(6)	2.345(6)	2.315(6)
M1–O3 x3	2.012(5)	2.011(4)	2.001(4)
M1–O4 × 3	2.068(5)	2.057(5)	2.061(5)
M2–O3 × 2	1.994(5)	1.972(4)	1.960(4)
M2–O2 × 2	2.017(5)	2.009(5)	1.990(5)
M2–O1 × 2	2.022(4)	2.002(4)	1.974(3)
M3–O2 × 6	2.027(5)	2.007(5)	1.977(5)
M4–O3 × 4	1.9989(5)	1.985(4)	1.978(4)
M4–O1 × 2	2.017(6)	2.001(6)	1.982(5)
M1–M1[a]	2.692(1)	2.702(1)	2.704(1)

[a] This M–M distance across the face shared octahedra has increased to 2.785(8) Å in $Pb_3Mn_7O_{15}$ [4].

Table 2
Atomic coordinates and isotropic displacement factors (Å$^2 \times 10^3$).

	$Pb_3Rh_{5.93}Mn_{1.07}O_{15}$				$Pb_3Rh_{4.74}Mn_{2.26}O_{15}$			
	x	y	z	U(eq)[a]	x	y	z	U(eq)[a]
Pb1	0	0.3926(1)	1/4	8(1)	0	0.3894(1)	1/4	10(1)
Pb2	0.7374(1)	0	1/4	6(1)	0.7388(1)	0	1/4	8(1)
M1	2/3	1/3	0.1487(1)	3(1)	2/3	1/3	0.1490(1)	4(1)
M2	0.6639(1)	0.1681(1)	0	4(1)	0.6645(1)	0.1677(1)	0	4(1)
M3	0	0	0	4(1)	0	0	0	6(1)
M4	1/2	0	0	3(1)	1/2	0	0	5(1)
O1	0.6666(5)	0	0.0780(5)	7(1)	0.6673(5)	0	0.0764(4)	9(1)
O2	0.8321(5)	0.1679(5)	0.0772(4)	7(1)	0.8332(5)	0.1668(5)	0.0763(4)	9(1)
O3	0.8418(4)	0.3337(4)	0.0808(3)	8(1)	0.8423(4)	0.3329(4)	0.0815(3)	8(1)
O4	0.5205(6)	0.3430(6)	1/4	5(1)	0.6557(6)	1749(6)	1/4	7(1)

[a] U(eq) is defined as one third of the trace of the orthogonalized U^{ij} tensor.

all four of the crystallographically distinct M octahedra as shown in Fig. 3. Thus, we also have a decrease in unit cell volume with increasing Mn content (Fig. 2). Given that all of these M–O bond distances have nearly equal contributions perpendicular and parallel to the *c* axis, we might expect that both *a* and *c* would decrease with increasing Mn content. In fact, *a* and *b* decrease with increasing Mn, but *c* increases. The M–M distances across the edge shared octahedra are all decreasing with decreasing Mn content because they have a component only perpendicular to the *c* axis. The M–M distances across the face shared octahedra, however, show an increase as the Mn concentration increases (Table 4), and this distance is aligned along the *c* axis. This then could be a partial explanation for the increase in *c* as the Mn content increases. However, this increase in this M–M distance is only significant for the pure Mn phase, and the increase in *c* actually occurs over the entire solid solution (Fig. 2). The answer to this increase in *c* lies with the Pb–O bonding (Fig. 6). As the M–O sheets contract in the *ab* plane with increasing Mn content, all the Pb–O4 distances in this plane decrease (Table 4 and Fig. 6). To compensate for this additional bonding power, the Pb–O distances that are essentially perpendicular to the *ab* plane (Pb1–O3 and Pb2–O1) increase (Table 4 and Fig. 6) resulting in an increase of *c*. There is another reason why the Pb–O bonding causes an increase in *c*. As the O atoms in the sheets become closer to one another with increasing Mn content, the O3–Pb1–O3 bond angles to the sheets are forced to decrease. The decrease of this angle from 66.2° to 63.0° on going from $Pb_3Rh_7O_{15}$ to $Pb_3Rh_{4.74}Mn_{2.26}O_{15}$ without any change in Pb–O distances would force an increase of 0.14 Å in *c*. Thus, the M–O sheets would be forced further apart even with no change in Pb–O distances. The M–O sheets themselves contract with increasing Mn content mainly perpendicular to *c* with little variation along *c* due to a constraint caused by the edge sharing of the octahedra [10].

Refinements of the Rh/Mn ratio at each of the four crystallographic sites show that Rh has a very strong preference for the 8*h* site (Table 3). This is the site where two octahedra share a face, and thus the site of maximum M–M repulsion. Bond valence

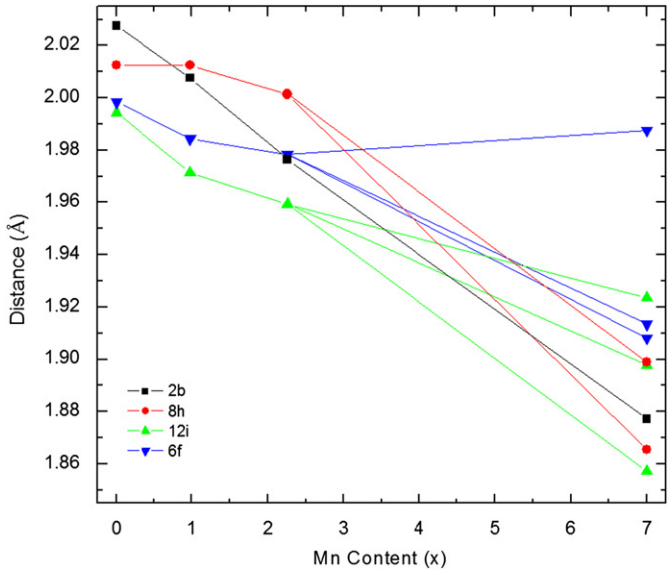

Fig. 3. Some interatomic distances (Rh/Mn–O) vs. *x* for $Pb_3Rh_{7-x}Mn_xO_{15}$ phases. $x<7$ phases are shown in hexagonal symmetry while the x=7 phase is shown in orthorhombic symmetry.

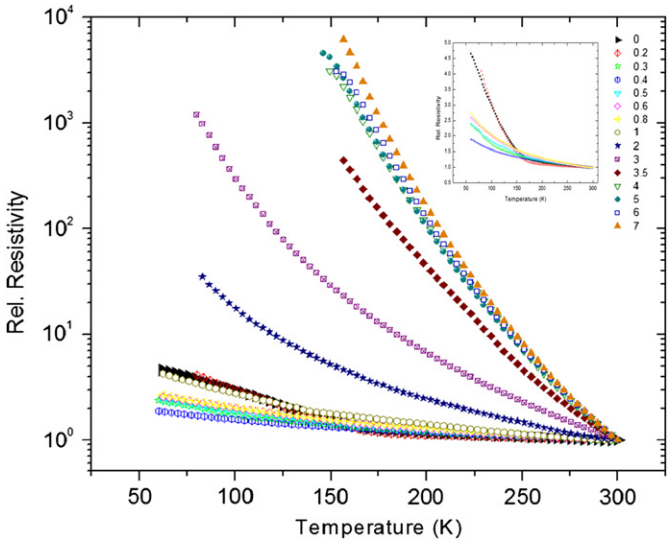

Fig. 4. Resistivity vs. temperature for $Pb_3Rh_{7-x}Mn_xO_{15}$ phases. Inset shows linear data for the $x<1$ phases.

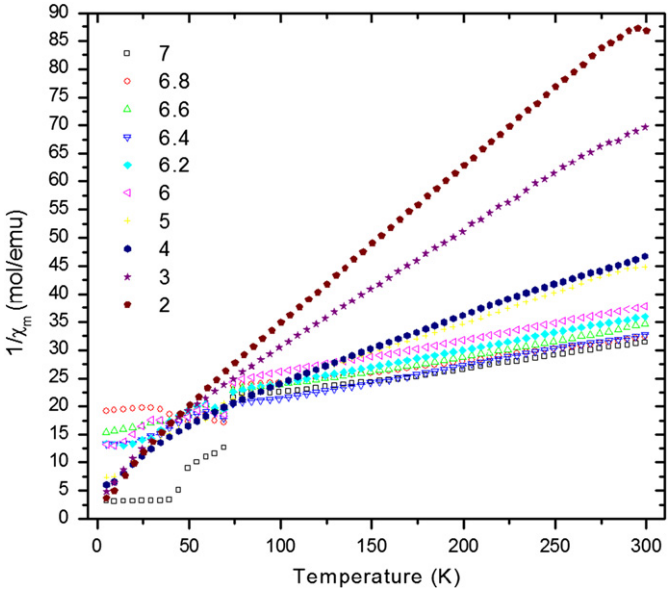

Fig. 5. Magnetic susceptibility for $Pb_3Rh_{7-x}Mn_xO_{15}$ phases. χ_m is calculated in emu/mol.

Table 5
Summary of magnetic susceptibility measurements for $Pb_3Rh_{7-x}Mn_xO_{15}$ phases.

	$Pb_3Rh_{7-x}Mn_xO_{15}$ effective paramagnetic moment data										
x	1	2	3	4	5	6	6.2	6.4	6.6	6.8	7
θ_w (K)	−7.5	−25.1	−58.6	−128.1	−126.8	−346.8	−303.6	−259.9	−338.9	−509.7	−390.2
C	1.61	3.59	5.06	9.08	9.37	17.15	16.75	16.86	18.62	25.19	22.03
μ_{obs} (m_B)	3.6	5.38	6.39	8.56	8.69	11.76	11.62	11.66	12.26	14.25	13.33

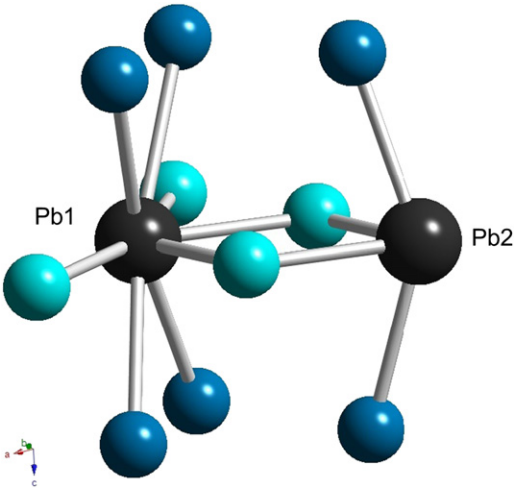

Fig. 6. Pb–O bonding in $Pb_3Rh_{7-x}Mn_xO_{15}$ phases. Contraction of *a* with increasing *x* causes Pb–O distances in the *ab* plane to decrease, which is compensated by an increase in Pb–O bond lengths perpendicular to this plane resulting in an expansion of *c*. The decrease of the O3–Pb1–O3 angle with increasing *x* also contributes to an increase in *c*.

calculations for $Pb_3Rh_7O_{15}$ show that this site is Rh^{3+} [7], as would be expected because the presence of Rh^{4+} would increase the electrostatic repulsion. Similarly, bond valence calculations for $Pb_3Mn_7O_{15}$ indicate an oxidation state close to 3+ for Mn at this site [4]. However, this M–M electrostatic repulsion depends on real charges, which are very different than oxidation states. Given the electronegativity values of 2.28 and 1.56 for Rh and Mn [11], respectively, the real positive charge for Rh^{3+} will be much less than that of Mn^{3+}. Thus, the electrostatic repulsion for Rh^{3+}–Rh^{3+} will be much less than for Mn^{3+}–Mn^{3+}, and this is reflected in the relevant distances of 2.69 Å for Rh^{3+}–Rh^{3+} and 2.78 Å for Mn^{3+}–Mn^{3+}. This much greater Mn^{3+}–Mn^{3+} distance relative to the Rh^{3+}–Rh^{3+} distance occurs despite the fact that Mn–O distances are considerably shorter than the Rh–O distances. This higher repulsion for Mn^{3+}–Mn^{3+} relative to Rh^{3+}–Rh^{3+} is then the explanation for the tendency of Mn to avoid this site in the solid solution (Table 3).

Our electrical resistivity measurements (Fig. 4) show that very little Mn substitution destroys the Verwey-type transition of $Pb_3Rh_7O_{15}$. The transition is evident for 3% substitution but has disappeared for 4% substitution. This demonstrates the very fragile nature of the charge ordering in $Pb_3Rh_7O_{15}$. The Verwey-type transition in Fe_3O_4 is also very sensitive to substitution for Fe. Substitutions for Fe of 2% Ni, Co, Al, Cr, or Ti result in a significant drop in the transition temperature [12]. Even a substitution of only 0.3% Ga gives a detectable change.

The magnetic properties of $Pb_3Mn_7O_{15}$ using a single crystal have been reported and analyzed in detail [8]. Paramagnetism is observed above 250 K, and there are several magnetic transitions below 250 K. The first at about 250 K was interpreted as short-range antiferromagnetic ordering within the layers only. Then at 70 K long-range, three-dimensional order occurs. Although this is basically antiferromagnetic ordering, weak ferromagnetism results due to an incomplete cancellation of spins. Finally, at 20 K there is another transition that has been interpreted as a reorientation of the spins. Our magnetic susceptibility data for polycrystalline $Pb_3Mn_7O_{15}$ (Fig. 5) are in general agreement with that reported. We see no clear evidence for a transition at about 250 K, but that transition was reported to give only a small change in slope of the $1/\chi$ curve vs. temperature curve. We see the sharp drop in $1/\chi$ at about 70 K indicative of long range magnetic order for all the samples up to and including $Pb_3Rh_3Mn_4O_{15}$ but not for samples richer in Rh.

Acknowledgments

Single crystal X-ray diffraction analysis was provided by L. Zakharov. This work was supported by NSF Grant DMR 0804167.

Appendix A. Supplementary material

Crystallographic information files (cif) can be found in the online version.

Supplementary data associated with this article can be found in the online version at doi:10.1016/j.jssc.2010.02.008.

References

[1] B. Darriet, M. Devalette, B. Latourrette, Acta Crystallogr. Sect. B: Structural Crystallography and Crystal Chemistry B 34 (1978) 3528.
[2] R.E. Marsh, F.H. Herbstein, Acta Crystallogr. Sect. B: Structural Science B 39 (1983) 280.
[3] Y. Le Page, L.D. Calvert, Acta Crystallogr. Sect. C: Crystal Structure Communications C 40 (1984) 1787.
[4] J.C.E. Rasch, D.V. Sheptyakov, J. Schefer, L. Keller, M. Boehm, F. Gozzo, N.V. Volkov, K.A. Sablina, G.A. Petrakovskii, H. Grimmer, K. Conder, J.F. Loeffler, J. Solid State Chem. 182 (2009) 1188.
[5] A.W. Sleight, H.-Y. Chen, J.L. Gillson, in: ACS/CSJ Chemical Congress, Honolulu, HI, April 1–6, 1979, American Chemical Society, Washington, DC, 1979, p. 75.
[6] P.J. Omaly, R. Kohlmuller, P. Batail, R. Chevalier, Acta Crystallogr. Sect. B 36 (1980) 1040.
[7] H. Mizoguchi, A.P. Ramirez, T. Siegrist, L.N. Zakharov, A.W. Sleight, M.A. Subramanian, Chem. Mater. 21 (2009) 2300.
[8] N.V. Volkov, K.A. Sablina, O.A. Bayukov, E.V. Eremin, G.A. Petrakovskii, D.A. Velikanov, A.D. Balaev, A.F. Bovina, P. Boni, E. Clementyev, J. Phys.: Condens. Matter 20 (2008) 055217.
[9] N.V. Volkov, K.A. Sablina, E.V. Eremin, P. Boni, V.R. Shah, I.N. Flerov, A. Kartashev, J.C.E. Rasch, M. Boehm, J. Schefer, J. Phys.: Condens. Matter 20 (2008) 445214.
[10] N. Khosrovani, A.W. Sleight, Int. J. Inorg. Mater. 1 (1999) 3.
[11] A.L. Allred, J. Inorg. Nucl. Chem. 17 (1961) 215.
[12] Y. Miyahara, J. Phys. Soc. Japan 32 (1972) 629.